

Electromagnetic modeling of stress corrosion cracks in Inconel welds

Haoyu HUANG¹, Noritaka YUSA^{2,*}, Kenzo MIYA¹, Hidetoshi HASHIZUME², Takehiko SERA³, and Shinro HIRANO³

¹ IJU Corp, 2-7-17-707, Ikenohata, Taito, Tokyo, 110-0008, Japan

² Department of Quantum Science and Energy Engineering, Graduate School of Engineering, Tohoku University, 6-6-01-2 Aramaki Aza Aoba, Aoba-Ku, Sendai, Miyagi, 980-8579, Japan

³ Kansai Electric Power, 13-8, Goichi, Mihama, Mikata, Fukui, 919-1141, Japan

ABSTRACT

This study evaluates suitable numerical modeling of stress corrosion cracks appearing in Inconel welds from the viewpoint of electromagnetic nondestructive evaluations. The stress corrosion cracks analyzed in this study are five artificial ones introduced into welded flat plate, and three natural ones found in a pressurized nuclear power plant. Numerical simulations model a crack as a planar region having a uniform conductivity inside and a constant width, and evaluate the width and conductivity that reproduce the maximum eddy current signals obtained by experiments. The results obtained validate the existence of the minimum value of the equivalent resistance, which is defined by the width divided by conductivity. In contrast, the values of the width and conductivity themselves vary across a wide range. The results also lead to a discussion about (1) the effect of probe utilized on the numerical model, (2) the difference between artificial and natural stress corrosion cracks, and (3) the difference between stress corrosion cracks in base metals and those in Inconel welds in their models. Electromagnetic characteristics of four different Inconel weld alloys are additionally evaluated using a resistance tester and a vibrating sample magnetometer to support the validity of the numerical modeling and the generality of results obtained.

KEYWORDS

electromagnetic nondestructive evaluation, eddy current testing, nuclear power plant, nickel-based alloy, finite element method, numerical modeling, natural crack, inverse problem, Alloy 600

ARTICLE INFORMATION

Article history:
Received 16 September 2010
Accepted 4 February 2011

1. Introduction

The emergence of stress corrosion cracks is one of the most important issues for the maintenance activity of aging nuclear power plants [1] [2]. The nondestructive evaluation of structures plays one of the most important roles in dealing with the problems related to stress corrosion cracks, as well as the development of technologies to prevent the initialization of such cracks. That is to say, taking a suitable maintenance action requires finding a stress corrosion crack in its initial state and evaluating its profile precisely to discuss its effect on structural integrity.

Usually, ultrasonic inspections are used in the evaluation of cracks found in nuclear power plants. However, the complexity and diversity of structures in nuclear power plants imply that it is preferable not to depend only on ultrasonic-based techniques. Several studies such as [3] have discussed the application of non-ultrasonic tests to the sizing of cracks to which it is difficult to apply ultrasonic tests. Eddy current testing is a promising nondestructive testing method from this point of view [4]. In addition to a large number of studies dealing with ideal cracks [5], recent studies have even reported the success of sizing stress corrosion cracks from measured eddy current signals using computational inversion techniques [6] [7] [8].

In contrast, however, another recent study has pointed out that conventional techniques developed to deal with ideal cracks are not always suitable for considering stress corrosion cracks [9]. One of the main reasons for this is that a numerical model suitable for dealing with a stress corrosion crack in

*Corresponding author, E-mail: noritaka.yusa@gse.tohoku.ac.jp

numerical simulations has not been established. Whereas a stress corrosion crack should be modeled not as an insulating wall or nonconductive region but as a region with a certain conductivity inside [6] [10], more specific information such as the amount of conductivity to model a stress corrosion crack has not been obtained so far. Earlier studies by the authors have revealed that it is necessary to take not only conductivity but also the width of a crack region explicitly into consideration to model a stress corrosion crack [11]. In addition, they also report that whereas the values of conductivity and width to model stress corrosion cracks vary across a wide range, it would be reasonable to assume the minimum value of the equivalent resistance, which is defined as the width divided by the conductivity. The existence of the minimum value of the equivalent resistance enables one to impose a constraint on the numerical inversion to evaluate crack profiles from eddy current signals, and thus should enable the problem to be properly considered. However, the earlier studies have considered only stress corrosion cracks in base metals. Recent experiences show that stress corrosion cracks tend to appear especially in Inconel welds. Thus discussions on the numerical modeling of stress corrosion cracks appearing in Inconel welds are indispensable from the viewpoint of the maintenance of nuclear power plants.

This study was conducted with the above background. The numerical models of five artificial stress corrosion cracks are discussed on the basis of their eddy current signals and the true profiles of the cracks revealed by destructive tests. This study also evaluates three natural stress corrosion cracks found in actual nuclear power plants. The validity of the assumptions, as well as the difference between the artificial and natural cracks, are discussed.

2. Evaluation of the electromagnetic characteristics of Inconel welds for the discussion of numerical modeling

Since a variety of Inconel weld metals are utilized in actual nuclear power plants, this study first evaluated the electromagnetic characteristics of four Inconel welds to discuss a suitable computational model and also to support the generality of the results obtained through this study. The welds evaluated and their AWS standard number are TR-52 (ERNiCrFe-7), NIC-70A (ENiCrFe-1), WEL TIG S82 (ERNiCr-3), and TGS-70Ncb (ERNiCr-3).

Welded plate specimens were prepared to evaluate the electromagnetic characteristics of each weld metal. The numbers of plate specimens to evaluate the electromagnetic characteristics of TR-52, NIC-70A, WEL TIG S82, and TGS-70Ncb were three, unity, unity, and unity, respectively (six welded plates in total).

Columnar samples were cut from the plate specimens to measure the conductivity of the weld metals. Each plate specimen provided two columnar samples with a diameter of 5 mm and a length of 90 mm. The resistance of the columnar samples was measured using a resistance tester (Resistance HiTester 3541, HIOKI E.E. Corp.), and the conductivity of the weld metals was calculated from the dimension of the samples and the distance between the terminals of the measurements. Table 1 summarizes the results of the measurement of the conductivity. The table shows that all the Inconel welds are less conductive than Inconel 600 base metal [14], which agrees with other reports [15] [16].

After measuring the conductivity, spherical samples were cut from the columnar samples to measure the relative permeability of the weld metals. Each columnar sample provided two spherical samples with a diameter of 4 mm. The B-H curves of the samples were measured using a vibrating sample magnetometer (VSM5-15, Toei Industry Co., LTD.). Table 2 summarizes the relative permeability of the weld metals calculated as $(dB/dH)/\mu_0$ at $H=0$, where μ_0 denotes the permeability of vacuum. The table shows that the values of relative permeability of all the welds are almost unity. In addition, all the samples did not show clear hysteresis or nonlinearity, as exemplified in Fig. 1.

The experimental results confirm that the difference between the four weld metals in their electromagnetic characteristics is not significant from the viewpoint of electromagnetic nondestructive evaluation. It is also reasonable to regard Inconel welds as a nonmagnetic material with a uniform conductivity in numerical simulations. It should be noted, however, that the electromagnetic characteristics evaluated here are rather macroscopic ones averaged over the samples. This indicates that noise due to Inconel welds stems from non-uniform distribution of electromagnetic characteristics, and thus the two conclusions above are valid only if signals are calibrated properly and noise due to the weld is negligible.

Table 1 Results of the measurement of conductivity of Inconel welds

| Weld metal | Welded Plate ID | Columnar Sample ID | Conductivity (MS/m) |
|-------------|-----------------|--------------------|---------------------|
| TR-52 | 1 | 1-1 | 0.90 |
| | | 1-2 | 0.90 |
| | 2 | 2-1 | 0.90 |
| | | 2-2 | 0.90 |
| | 3 | 3-1 | 0.90 |
| | | 3-2 | 0.90 |
| NIC-70A | 4 | 4-1 | 0.94 |
| | | 4-2 | 0.94 |
| WEL TIG S82 | 5 | 5-1 | 0.89 |
| | | 5-2 | 0.89 |
| TGS-70Ncb | 6 | 6-1 | 0.88 |
| | | 6-2 | 0.88 |

Table 2 Results of the measurement of relative permeability of Inconel welds

| Weld metal | Columnar Sample ID | Relative permeability of spherical sample 1 | Relative permeability of spherical sample 2 |
|-------------|--------------------|---|---|
| TR-52 | 1-1 | 1.00 | 1.00 |
| | 1-2 | 1.00 | 1.00 |
| | 2-1 | 1.00 | 1.00 |
| | 2-2 | 1.00 | 1.00 |
| | 3-1 | 1.00 | 1.00 |
| | 3-2 | 1.00 | 1.00 |
| NIC-70A | 4-1 | 1.01 | 1.01 |
| | 4-2 | 1.01 | 1.01 |
| WEL TIG S82 | 5-1 | 1.00 | 1.01 |
| | 5-2 | 1.00 | 1.00 |
| TGS-70Ncb | 6-1 | 1.00 | 1.00 |
| | 6-2 | 1.00 | 1.00 |

3. Evaluation of the numerical model of stress corrosion cracks in Inconel welds

3.1 Preparation of specimens

This study fabricated five welded plate specimens, whose dimensions are illustrated in Fig. 2, in order to discuss numerical modeling of stress corrosion cracks in Inconel welds. The specimen was a flat plate made of type 304 and type 316L stainless steel plates butt welded using NIC-70A. The surface of the weld was ground flat after welding. A stress corrosion crack was artificially introduced by imposing tensile stress on the surface using a three-point bending jig and soaking in a polythionic acid solution. Table 3 presents the widths of the weld, which is denoted as w in Fig. 2.

3.2 Eddy current inspection

Eddy current inspections were carried out using a commercial eddy current instrument (aect2000s, ASWAN Co. Ltd.,) to gather eddy current signals due to the cracks. Four eddy current probes were used: a differential type plus point probe for high frequencies, a differential type plus point probe for lower frequencies, an absolute type pancake probe for higher frequencies, and an absolute type pancake probe for lower frequencies. The square coils forming the plus point probes measured 10×10 mm and 4.4×4.4 mm in outer and inner squares and 3.6 mm in width. The pancake

probes had 5 and 1.6 mm in outer and inner diameters and were 2 mm in height. The probes for higher frequencies were driven at 100, 200, and 400 kHz; those for lower frequencies were at 25, 50, and 100 kHz. The probes were positioned precisely by an automated XY stage and two-dimensionally scanned the surface of the specimens. Signals gathered were recorded by a PC through an AD converter (NR-2000, Keyence Corporation).

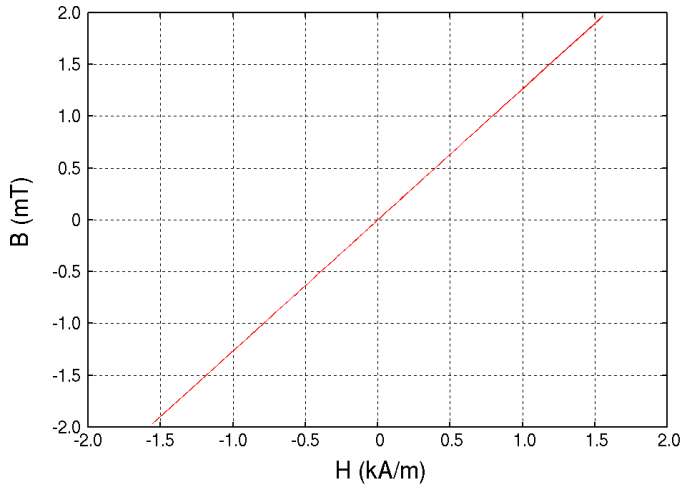


Fig. 1. B-H curve of NIC-70A weld metal

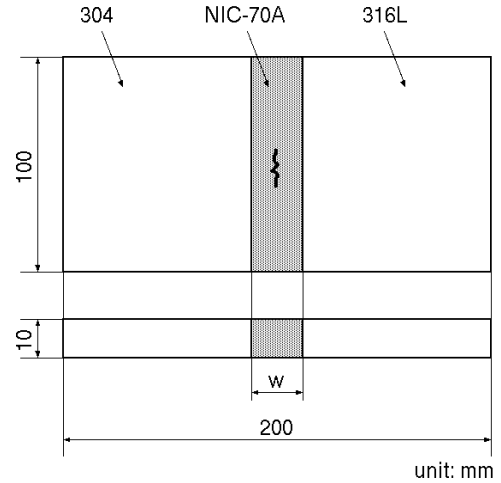


Fig. 2. Plate specimen with artificial stress corrosion cracks

Table 3 Widths of the weld lines of the specimens

| Specimen ID | Width of weld line, w (mm) |
|-------------|----------------------------|
| TP1 | 35 |
| TP2 | 35 |
| TP3 | 45 |
| TP4 | 45 |
| TP5 | 45 |

Measured signals were calibrated using signals due to an artificial rectangular slit introduced into a flat plate made from Inconel 600 base metal. The slit was 10 mm in long, 5 mm deep and 0.3 mm wide. Then simple spatial filters to eliminate uniform noise were imposed on the measured signals as

$$\mathbf{V}^x(x,y) = \mathbf{V}(x,y) - \mathbf{V}(x_s,y) - (\mathbf{V}(x_e,y) - \mathbf{V}(x_s,y)) \frac{(x-x_s)}{(x_e-x_s)}, \quad (1)$$

$$\mathbf{V}^y(x,y) = \mathbf{V}(x,y) - \mathbf{V}(x,y_s) - (\mathbf{V}(x,y_e) - \mathbf{V}(x,y_s)) \frac{(y-y_s)}{(y_e-y_s)}, \quad (2)$$

where $\mathbf{V}(x,y)$ is a two-dimensional vector consisting of the X- and Y-components of the measured signals. Variables x and y indicate the probe position at which the signals were measured; x and y are perpendicular and parallel to the weld line. Subscripts s and e denote the minimum and maximum values of X and Y locations that the scan covers.

Figures 3 presents the distribution of eddy current signal amplitude obtained using the plus point probe for higher frequencies and the pancake probe for higher frequencies. The signals were obtained at 100 kHz; the amplitudes of the signals were normalized so that the maximum signal amplitude due to the slit was 10 V. The figure confirms that all the stress corrosion cracks provided clear signals. Signals obtained using the plus point probe exhibited several peaks in most cases, although those using the pancake probe provided only one peak approximately at the center of each crack. Since both the probes had almost the same dimensions and thus there should not be such a significant difference between their probes in their spatial resolutions, this implies that the stress corrosion cracks introduced in this study had a large equivalent conductivity and a large equivalent width as indicated in [17]. Signals obtained at other frequencies and other probes were qualitatively similar.

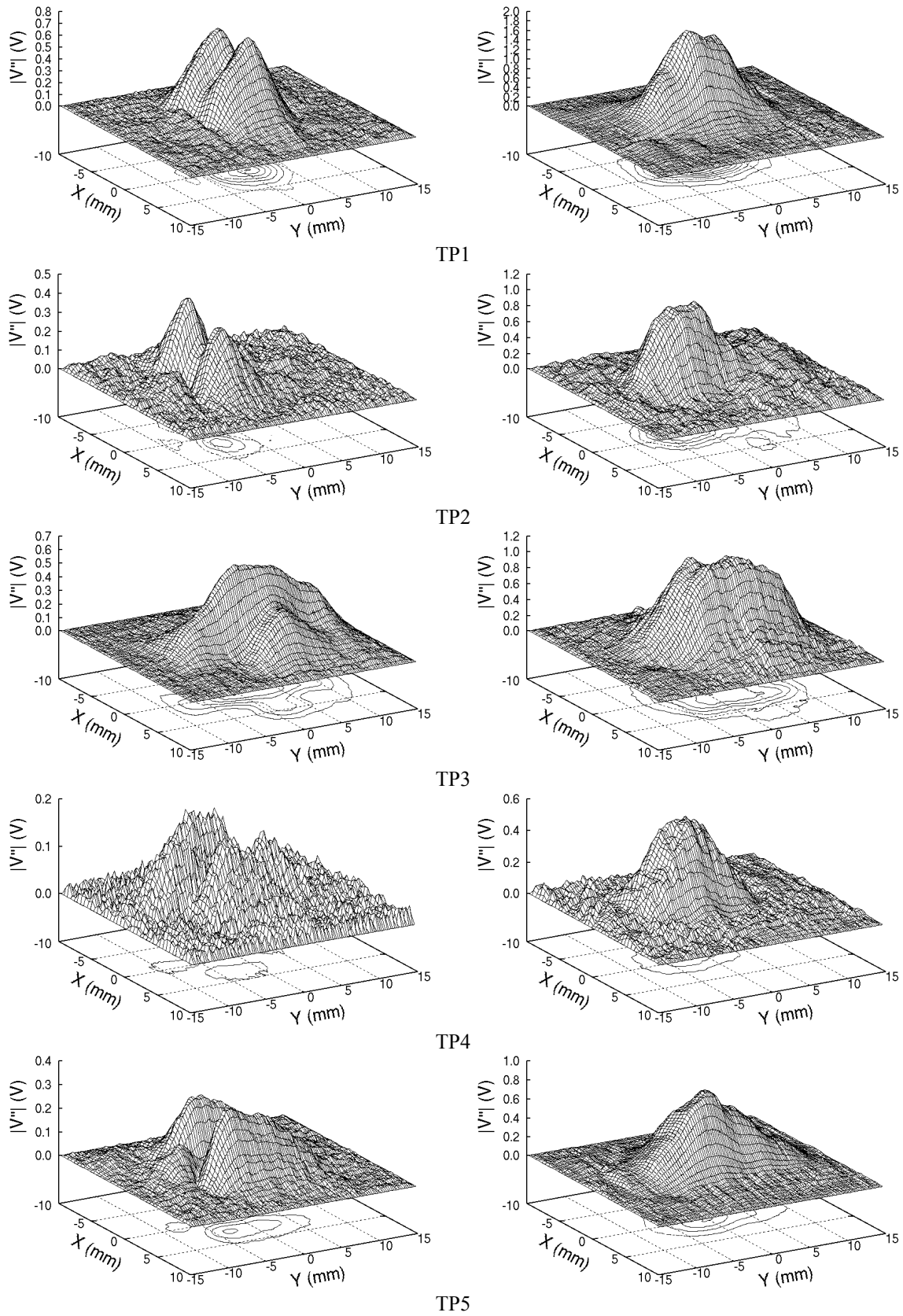


Fig. 3. Eddy current signals measured using the plus point probe (left) and pancake probe (right). The origin of the XY plane corresponds to the center of the specimen.

3.3 Destructive tests

After the eddy current tests, the specimens were destroyed to reveal the true profiles of the stress corrosion cracks. The destructive tests observed the cross-sectional profiles of the cracks at planes perpendicular to the weld lines. The distance between two neighboring planes was 2 mm.

Figures 4 and 5 show the cross-sectional profiles of the cracks observed at the center of the specimens and the boundary profiles of the cracks evaluated on the basis of the maximum depths of the cracks on each planes, respectively. The destructive tests revealed that the profiles of the introduced stress corrosion cracks are categorized into three types. That is,

- 1) TP1 and TP2 had planar cracks propagating mainly in depth direction. The cracks showed clearer crack openings than other specimens. TP2 contained one relatively long crack and a few shorter cracks running in parallel, and the maximum distance between them was about 1.3 mm.
- 2) TP3 contained quite a few small cracks running parallel to each other. The maximum distance between the cracks was as much as 10 mm.
- 3) TP4 and TP5 had single but quite volumetric cracks. Each specimen contained a single crack; the cracks propagated not only to the depth direction but also the horizontal direction of the specimen. Several cross-sectional planes, including the ones shown in Fig. 4, showed crack openings that were not connected to the surface of the specimen. This indicates that the cracks propagated inside the weld metal in a complicated fashion.

3.4 Numerical evaluation of the crack parameters and comparison with natural stress corrosion cracks found in Inconel welds of nuclear power plants

Finite element simulations were carried out to evaluate numerical models of the stress corrosion cracks. The computational model adopted in the simulations is illustrated in Fig. 6. A crack was modeled as an assembly of columnar regions embedded inside a flat plate with uniform electromagnetic characteristics of a conductivity of 0.94 MS/m and a relative permeability of 1. The depths of the columnar regions corresponded to the boundary profiles of the cracks revealed by the destructive tests; the columnar regions had a constant width, w , and uniform conductivity σ' . The number of columnar regions in crack width direction was unity and thus a crack was modeled as a planar region with a width of w .

The simulations were carried out using a finite element method-boundary element method eddy current simulator based on a time-harmonic A- ϕ formulation [18]. The maximum signal obtained by the numerical simulations was compared with that obtained by the experiments, and evaluated the equivalent width, w , and the equivalent conductivity, σ' , of a crack. Specifically, the numerical simulations were carried out using the parameters shown in Table 4, and signals at an arbitrary conductivity were calculated by interpolating the results of the numerical simulations. Then, w and σ' satisfying

$$|\mathbf{V}'' - \mathbf{V}_{\text{simu}}(w, \sigma')| / |\mathbf{V}''| \leq \varepsilon \quad (3)$$

were regarded as suitable parameters termed as equivalent width and equivalent conductivity, respectively in this study. Two-dimensional vectors \mathbf{V}'' and \mathbf{V}_{simu} were measured and simulated eddy current signals, and were calibrated using the signals due to the slit so that they were quantitatively comparable to each other. The threshold, ε , was set to 0.05 because of the presence of noise due to the weld. The evaluation took consideration of not only the maximum amplitude of signals but also its qualitative spatial distribution. That is, evaluation of the signals due to the plus point probes imposed such a constraint that whether a crack provided a single signal peak directly above the crack or two signal peaks appearing in the proximity of the crack, whereas the locations of the two peaks were not explicitly taken into consideration. It should be noted that the simulations considered only one crack although the destructive tests revealed some of the specimens contained multiple cracks.

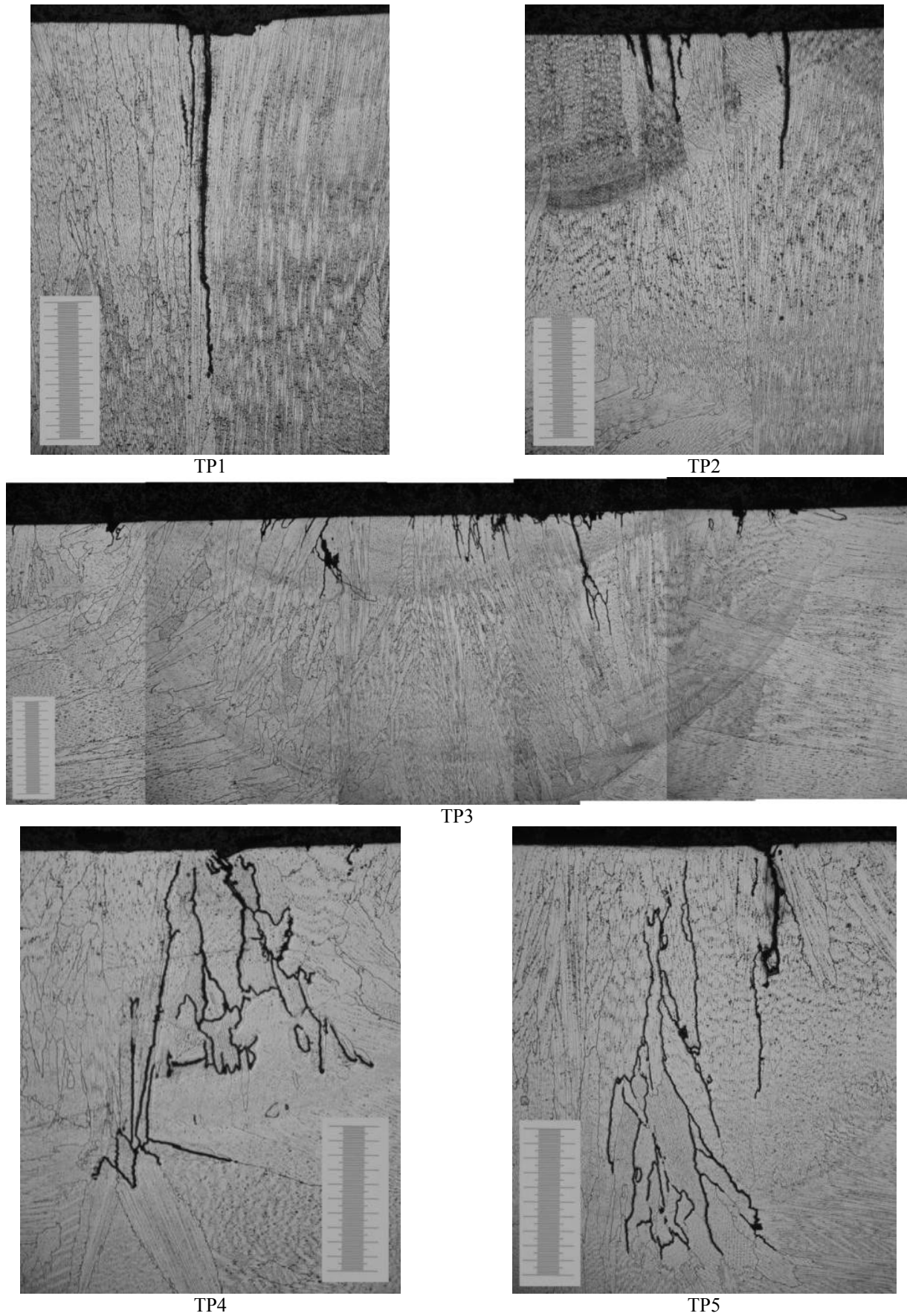


Fig. 4. Cross-sectional profiles of the cracks, observed at $Y=0$.

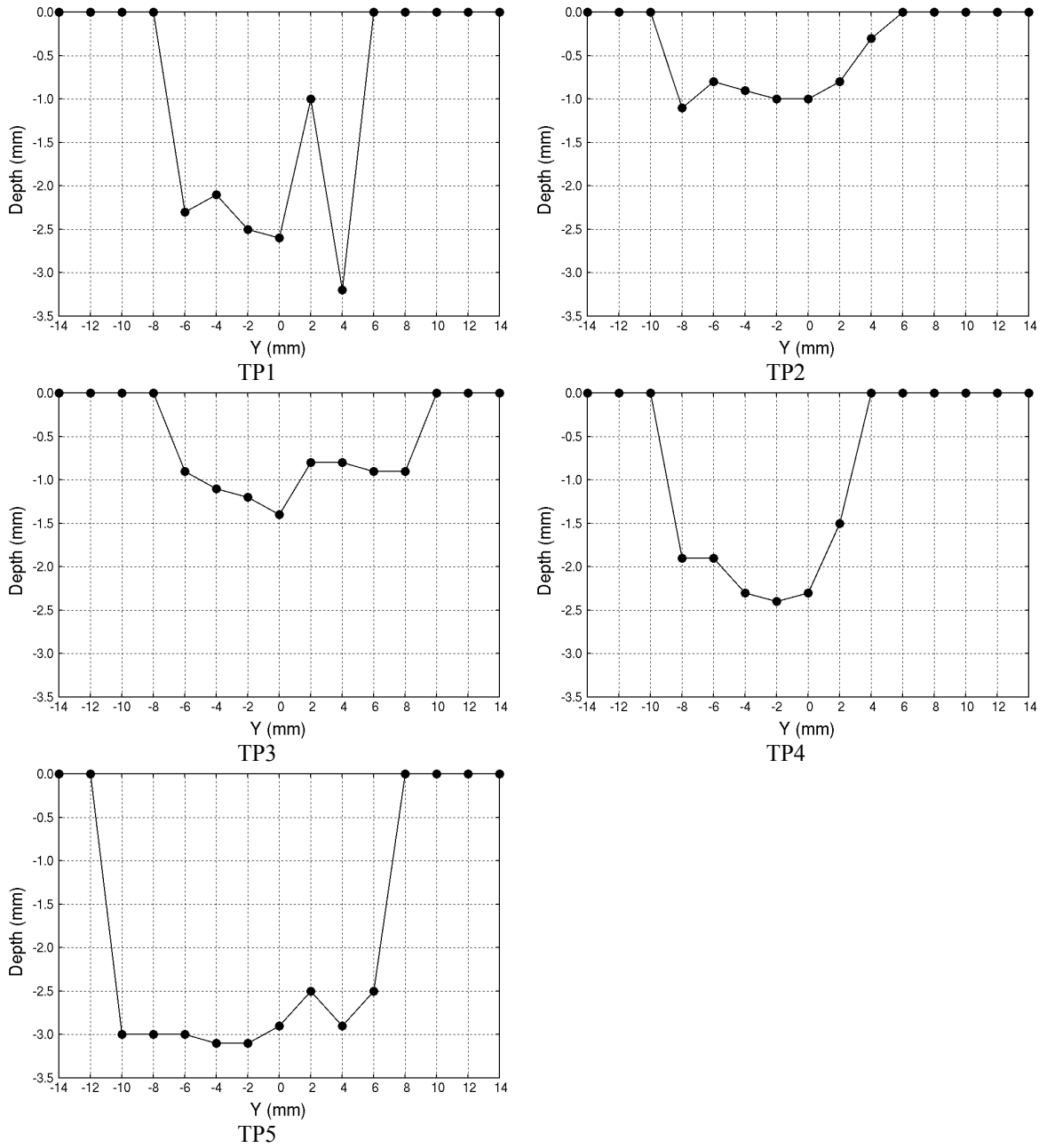


Fig. 5. The boundary profiles of the cracks. Black solid circles indicate the maximum depths of the cracks observed at each plane. The origin of the horizontal axis corresponds to the center of the specimen.

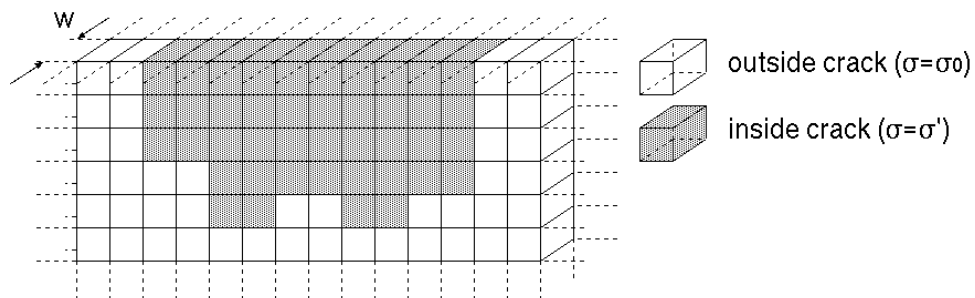


Fig. 6. Numerical modeling of the stress corrosion cracks. The conductivity of base material is denoted as σ_0 .

Table 4 Parameters utilized in the numerical simulations

| Parameter | Value |
|------------------------------|---|
| width, w (mm) | 0.01, 0.03, 0.05, 0.1, 0.3, 0.5, 1, 1.5, 2.0, 3.0, 4.0, 5.0 |
| conductivity, σ' (%)* | 0, 0.1, 0.3, 0.5, 1, 2, 5, 10, 15, 20, 30, 40, 50, 60, 70, 80, 90, 95, 99 |

* conductivity with respect to those of outside crack (σ_0)

Figures 7 and 8 summarize the results of the simulations to analyze signals obtained using the pancake probes and the plus point probes, respectively. The figures exclude cases that did not satisfy eqn. (3). That is, for example, Fig. 7 (a) excludes signals measured at 100 kHz using the low frequency pancake probe as well as those at 200 kHz using the high frequency pancake because the signals measured at these frequencies were not reproduced by the numerical simulation. In addition, signals due to TP2 measured by the pancake probes did not satisfy eqn. (3) at all the frequencies. The equivalent resistance of a crack, denoted as R in the figure, is defined as equivalent width divided by the equivalent conductivity [12]. The figures indicate that the equivalent width and equivalent conductivity of stress corrosion cracks vary significantly and therefore it would not be reasonable to assume their minimum and maximum values in modeling stress corrosion cracks. In contrast, the figures imply the validity of assuming the minimum equivalent resistance of stress corrosion cracks, which agrees well with the finding of an earlier study by the authors considering stress corrosion cracks in base metal. The results obtained by analyzing the signals obtained using the plus point probes are rather complicated. This is because the equivalent width of a crack has a significant effect on the characteristics of signals [17] [22]. Comparing the two figures indicates that the probe utilized had less effect on equivalent resistance of a crack than equivalent width and conductivity themselves.

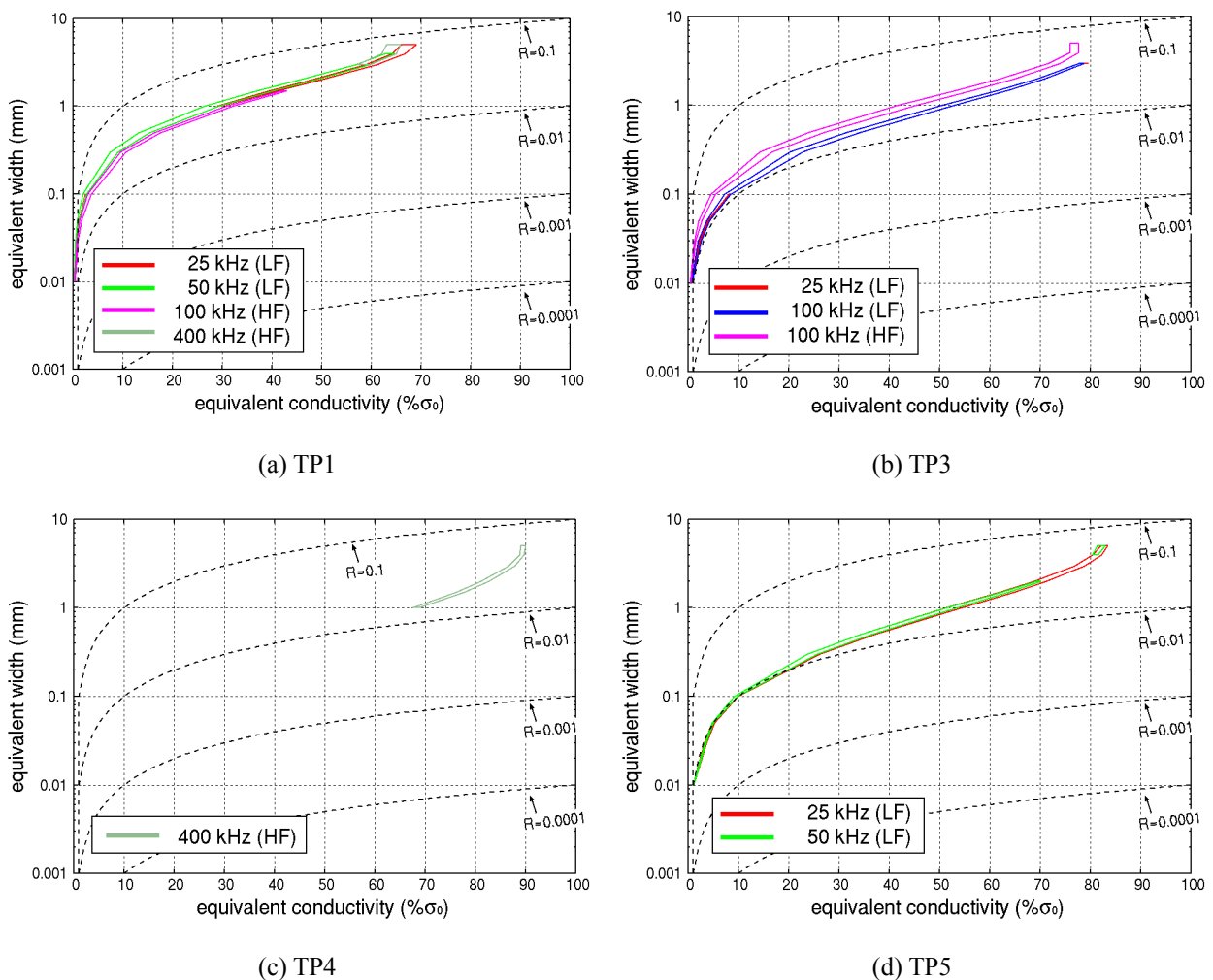


Fig. 7. Results of the numerical simulations to evaluate suitable model of the artificial stress corrosion cracks, when signals are measured by the pancake probes.

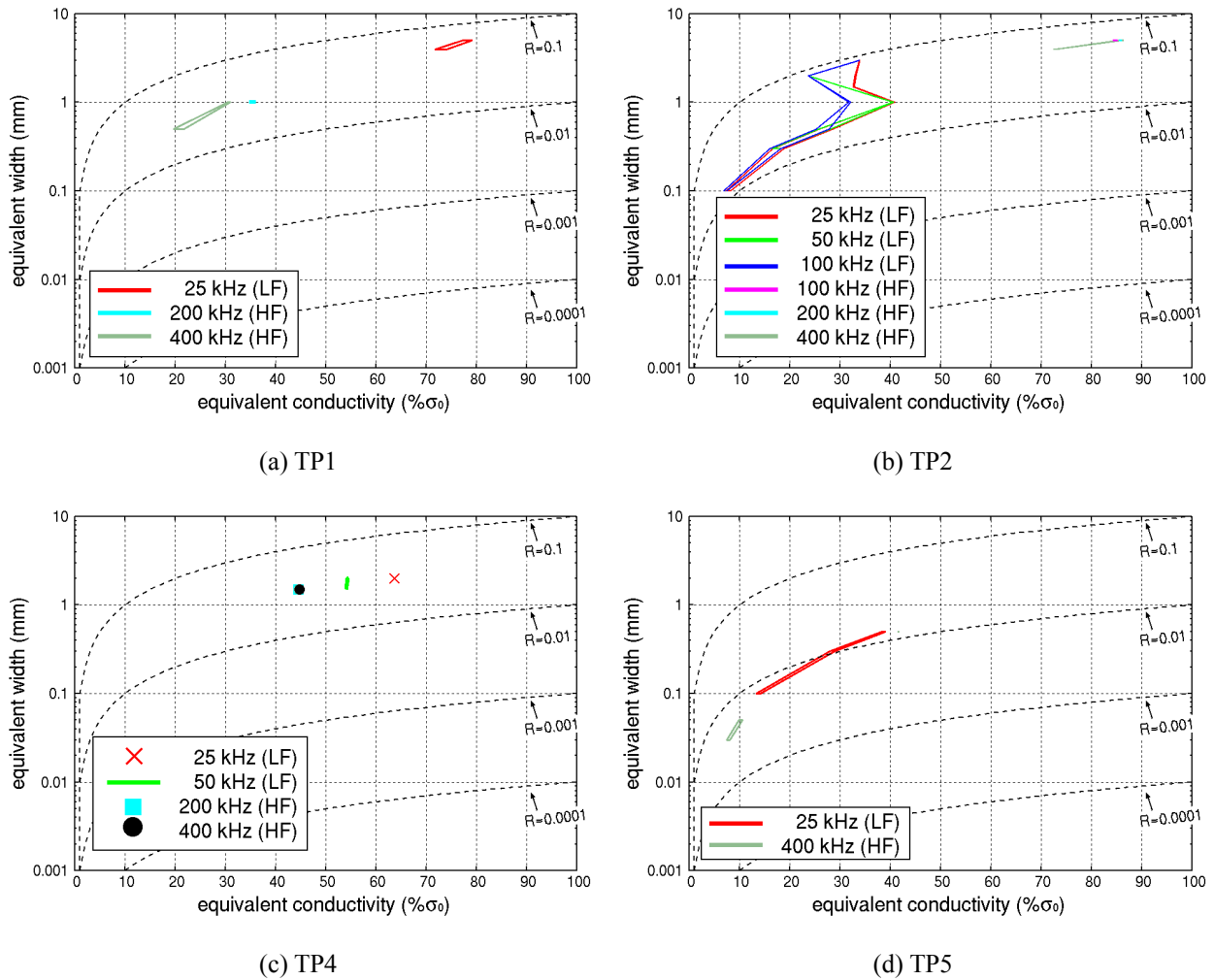


Fig. 8. Results of the numerical simulations to evaluate suitable model of the artificial stress corrosion cracks, when signals are measured by the plus point probe.

Figure 9 presents the results of the same analysis on three natural stress corrosion cracks found in Inconel welds of nuclear power plants, together with the maximum depth and length of each crack. Eddy current signals were obtained using a plus point probe; each crack was sufficiently separate from the others, and two-dimensional distribution of the measured signals showed only a single peak directly above the crack. This implies that the natural stress corrosion cracks were not volumetric like the artificial ones. Actually, the results presented in Fig. 9 indicate that the natural stress corrosion cracks should be modeled as a relatively thin region. The equivalent resistances of the natural stress corrosion cracks are somewhat smaller than those of the artificial ones.

Figure 10 shows the results of the earlier study analyzing stress corrosion cracks in base metals [13]. There is not such a significant difference between stress corrosion cracks in base metals and those in Inconel welds from the viewpoint of their equivalent resistance, whereas the results obtained in this study imply that stress corrosion cracks appearing in Inconel welds tend to have less equivalent resistance. It should be noted that the figure summarizes the results obtained by various eddy current probes, and parameters to model a stress corrosion crack depend on the probe utilized. Therefore systematically obtained data are needed for further quantitative discussion.

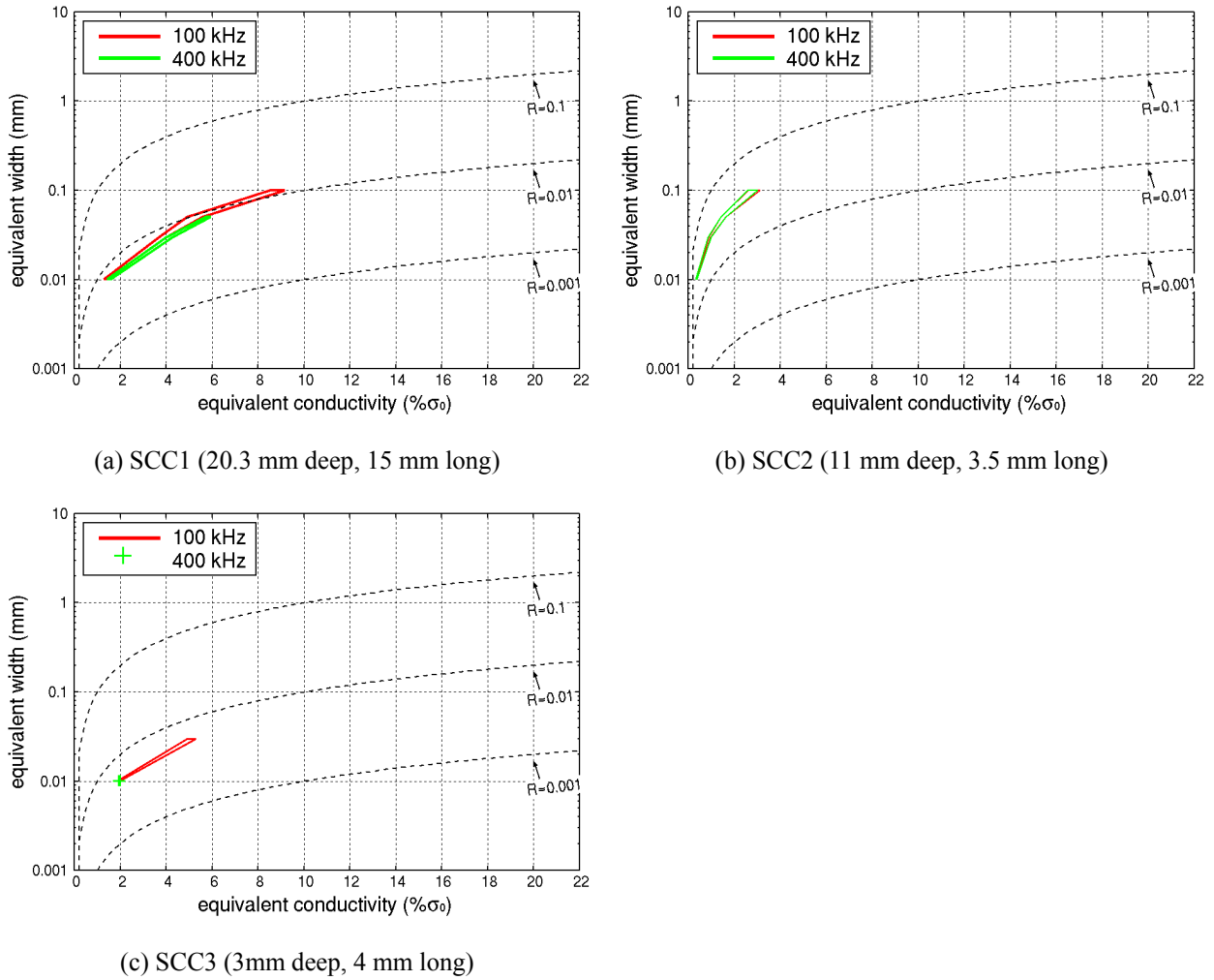


Fig. 9. Results of the numerical simulations to evaluate suitable model of the natural stress corrosion cracks.

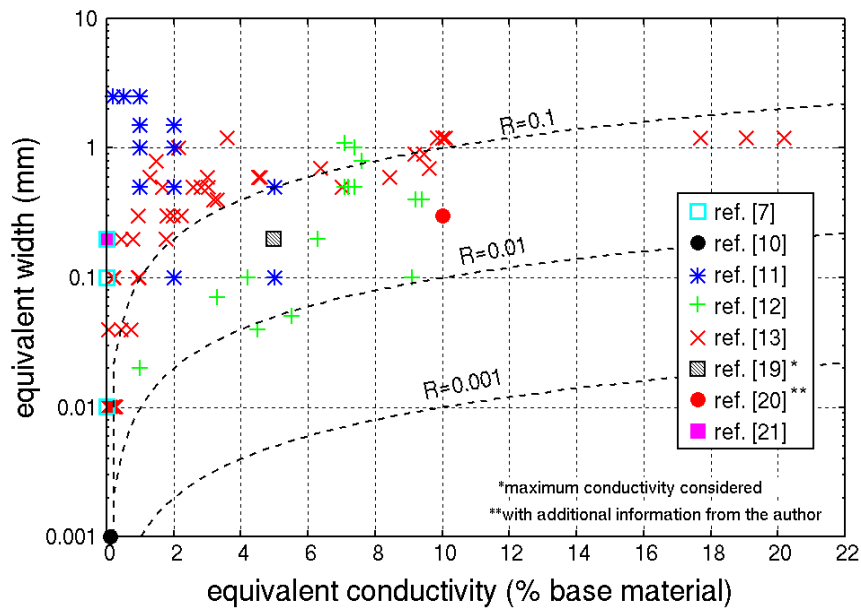


Fig. 10. Numerical models of stress corrosion cracks in base materials (originally presented in [13], used in this paper with a permission of copyright).

4. Conclusion

This study evaluated numerical modeling of stress corrosion cracks in Inconel welds. The study dealt with five artificial stress corrosion cracks introduced into Inconel welds, NIC-70A, and another three natural ones found in Inconel welds of actual power plants. A crack was modeled as a region having a constant width and uniform conductivity inside, and numerical simulations were carried out to evaluate the values of the width and conductivity. These simulations provided reasonable agreement between measured and simulated signals in their maximum signals.

- (1) When a stress corrosion crack is modeled as above, the width and conductivity of the modeled crack depend significantly on the probe and excitation frequency. However the equivalent resistance, which was defined as width divided by conductivity, depends much less on these factors.
- (2) The artificial stress corrosion cracks prepared in this study were more volumetric than natural ones. This is confirmed not only the results of destructive tests revealing their cross-sectional profiles; actually in the numerical model the artificial cracks were regions with relatively large width and large conductivity. However, there was no significant difference between their equivalent resistances.
- (3) The stress corrosion cracks in Inconel welds considered in this study tended to have less equivalent resistance than those in base metals.

Additional experiments were carried out to evaluate the electromagnetic characteristics of four Inconel weld metals. The experiments confirmed their differences were negligible from the viewpoint of eddy current testing, which supports the generality of the results obtained in this study. It should be noted that in this study Inconel welds were modeled as a non-magnetic region having a uniform conductivity. However, actually, the electromagnetic characteristics measured were averaged over a volume. It is quite likely that from a more microscopic point of view the weld has more distributed electromagnetic characteristics, which would be one of the reasons why the agreement between the experiments and simulations were not satisfactory in several cases.

Although earlier studies by the authors demonstrated that a crack model with a uniform conductivity inside provides good agreement when the maximum signals due to stress corrosion cracks in a base metal are considered [12] [13], this study sometimes failed to reproduce signals by numerical simulations using the model. The most plausible reason for this is that this study considered cracks in welds and signal processing adopted could not eliminate noise due to the weld sufficiently or modified signals due to the crack. It would be likely that more complicated crack modeling such as anisotropic conductivity [23] and three-dimensional modeling [24] would be necessary to deal with stress corrosion cracks in a general sense.

References

- [1] S. Suzuki, K. Takamori, K. Kumagai, A. Sakashita, N. Yamashita, C. Shitara, and Y. Okamura, Stress corrosion cracking in low carbon stainless steel components in BWRs, *E-Journal of Advanced Maintenance* 1 (2009), 1-29
- [2] H. Tanaka, Industry's efforts toward technology development related to aging management of PWR plants, *E-Journal of Advanced Maintenance* 1 (2010), GA10,.
- [3] I. Komura, T. Hirasawa, S. Nagai, J. Takabayashi, and K. Naruse, Crack detection and sizing technique by ultrasonic and electromagnetic method, *Nuclear Engineering and Design* 206 (2001), 351-362.
- [4] D. Horn and W.R. Mayo, NDE reliability gains from combining eddy-current and ultrasonic testing, *NDT&E International* 33 (2000), 351-362.
- [5] B.A. Auld and J.C. Moulder, Review of advances in quantitative eddy current nondestructive evaluation, *Journal of Nondestructive Evaluation* 18 (1999), 3-36.
- [6] N. Yusa, Z. Chen, K. Miya, T. Uchimoto, and T. Takagi, Large-scale parallel computation for the reconstruction of natural stress corrosion cracks from eddy current testing signals, *NDT&E International* 36 (2003), 449-459.
- [7] H. Huang and T. Takagi, Inverse analyses for natural and multicracks using signals from a differential transmit-receive ECT coil, *IEEE Transactions on Magnetics* 38 (2002), 1009-1012.

- [8] F. Kojima, N. Kubota, F. Kobayashi, and T. Takagi, Shape recovery of natural crack using evolutionary programming related to eddy current testing, *International Journal of Applied Electromagnetics and Mechanics* 15 (2001/2002), 243-247.
- [9] N. Yusa, L. Janousek, M. Rebican, Z. Chen, K. Miya, N. Dohi, N. Chigusa, and Y. Matsumoto, Caution when applying eddy current inversion to stress corrosion cracking, *Nuclear Engineering and Design* 236 (2006), 211-221.
- [10] Z. Badics, Y. Matsumoto, K. Aoki, F. Nakayasu, and A. Kurokawa, Finite element models of stress corrosion cracks (SCC) in 3-D eddy current NDE problems, in: *Nondestructive Testing of Materials*, R. Collins, W.D. Dover, J.R. Bowler, and K. Miya eds., IOS Press, Amsterdam, 1995, pp. 21-29.
- [11] N. Yusa, S. Perrin, K. Mizuno, and K. Miya, Numerical modeling of general cracks from the viewpoint of eddy current testing, *NDT&E International* 40 (2007), 577-583.
- [12] N. Yusa and K. Miya, Discussion on the equivalent conductivity and resistance of stress corrosion cracks in eddy current simulations, *NDT&E International* 42 (2009), 9-15.
- [13] N. Yusa and H. Hashizume, Evaluation of stress corrosion cracking as a function of its resistance to eddy currents, *Nuclear Engineering and Design* 239 (2009), 2713-2718.
- [14] T. Takagi and H. Fukutomi, Benchmark activities of eddy current testing for steam generator tubes, in: *Electromagnetic Nondestructive Evaluation (IV)*, S.S. Udpa, T. Takagi, J. Pavo, and R. Albanese, eds., IOS Press, Amsterdam, 2000, pp. 235-252.
- [15] L. Janousek, N. Yusa, Z. Chen, and K. Miya, Recognition of INCONEL weld conductivity variation by means of eddy current testing, in: *Electromagnetic Nondestructive Evaluation (VIII)*, T. Sollier, D. Premel, and D. Lesselier eds., IOS Press, Amsterdam, 2004, pp. 286-293.
- [16] W. Cheng, I. Komura, M. Shiwa, and S. Kanemoto, Eddy current examination of fatigue cracks in Inconel welds, *Journal of Pressure Vessel Technology* 129 (2007), 169-174.
- [17] Z. Chen, L. Janousek, N. Yusa, and K. Miya, A nondestructive strategy for distinction of natural fatigue and stress corrosion cracks based on signals of the eddy current testing, *Journal of Pressure Vessel Technology* 129 (2007), 719-728.
- [18] F. Matsuoka and A. Kameari, Calculation of three dimensional eddy current by FEM-BEM coupling method, *IEEE Transactions on Magnetics* 24 (1998), 182-185.
- [19] W. Cheng, S. Kanemoto, I. Komura, and M. Shiwa, Sizing of partial-contact stress corrosion cracks from ECT signals, *NDT&E International* 39 (2006), 374-383.
- [20] H. Endo, T. Uchimoto, T. Takagi, A. Nishimizu, M. Koike, and T. Matsui, Natural crack sizing based on eddy current image and electromagnetic field analyses, *Review of Progress in Quantitative Nondestructive Evaluation* 25 (2006), 720-727.
- [21] N. Yusa, Z. Chen, and K. Miya, Sizing of stress corrosion cracking on austenitic stainless piping in a nuclear power plant from eddy current NDT signals, *Nondestructive Testing and Evaluation* 20 (2005), 103-114.
- [22] S. Perrin, N. Yusa, and K. Miya, Automatic discrimination of stress corrosion and fatigue cracks using eddy current testing, in: *Electromagnetic Nondestructive Evaluation (V)*, S. Takahashi and H. Kikuchi, eds., IOS Press, Amsterdam, 2007, 91-98.
- [23] M. Tanaka, H. Tsuboi, Finite element model of natural crack in eddy current testing problem, *IEEE Transactions on Magnetics* 37 (2001), 3125-3128.
- [24] Y. Li, L. Udpa, and S. Udpa, Three-dimensional defect reconstruction from eddy-current NDE signals using a genetic local search algorithm, *IEEE Transactions on Magnetics* 40 (2004), 410-417.